A Theoretical Study of the Photoluminescence in the Eyes of Trilobites Under Natural Lighting and its Effect on Their Vision

SCOTT A. LEE[1], Department of Physics and Astronomy, University of Toledo, Toledo, OH, USA; ANNA ŻYLIŃSKA, University of Warsaw, Faculty of Geology, Warsaw, Poland; ROBERT W. COLLINS, Department of Physics and Astronomy, University of Toledo, Toledo, OH, USA.

ABSTRACT. Trilobites had a unique visual system in which the focusing component of their compound eyes were calcite crystals. Biogenic calcite emits photoluminescence (PL) in the blue-green part of the visual spectrum in all directions when excited by long-wavelength ultraviolet (UV-A) radiation. This PL had no information about the image being formed by the incident light from objects (such as other animals and rocks) near the trilobite and would have acted as stray light, thereby obscuring its vision. The PL spectrum from biogenic calcite from extant red algae is used to model the PL emitted by the calcite in the eyes of trilobites. The visible range and the wavelength sensitivity of the extant marine crustacean *Squilla empusa* (a distant living relative of the trilobites) is used to model the vision of trilobites. In the first theoretical calculation, the magnitude of this PL is estimated using data from extant red algae (including the concentration of its PL centers) and is compared to the expected photon noise in the visible sunlight directly from the illuminated objects. Due to the differences in the transmission of visible and UV-A light by seawater, PL stray light obscuration is expected to lessen with depth. A second more general calculation determines the dependence of this obscuration effect on ocean depth, independent of the concentration of PL centers in the calcite, showing that the obscuring effect of PL diminishes with depth. This PL is insignificant at 10 meters deep and, possibly, at all depths.

Publication Date: July 2025 **https://doi.org/10.18061/ojs.v124i2.9609** **OHIO J SCI 124(2):52-72**

INTRODUCTION

Trilobites were successful marine arthropods that lived throughout the Paleozoic Era. Their fossils are readily collected by both scientists and amateurs all around the world. For example, the Ohio state fossil is the Ordovician trilobite *Isotelus maximus* which belongs to some of the largest trilobites in the world (Rudkin et al. 2003; Brandt and Davis 2007). Trilobites first appear in the fossil record about 520 million years ago (MYA) and survived until the end-Permian Extinction 251 MYA (e.g., Whittington 1992; Schoenemann 2021). Most trilobites are considered to have lived on the bottom of the ocean (Bergström 1973; Fortey 2004) (Fig. 1) within the shelves of ancient continents, at almost every depth (even beyond the light range), resulting in a plethora of morphotypes and sizes (Fortey 2004). Some trilobites even had a pelagic or planktonic mode of life (McCormick and Fortey 1998; Schoenemann et al. 2010). Trilobites are believed to have fed mostly on edible detritus and organic particles extracted from sediment or suspension; however, both predatory and scavenging habits have been noted (Fortey and Owens 1999). The high preservation potential of trilobite fossils comes from the fact that their dorsal (back) exoskeleton was mineralized with calcite (set in an organic base). It is commonly considered that the trilobite cuticle was composed of low-magnesium calcite (Wilmot and Fallick 1989), although there is also evidence that some trilobites may have simultaneously crystallized high-magnesium calcite (Lee et al. 2012).

Though a few species of trilobites were blind, having lost eyesight due to evolution (see Schoenemann 2021 for overview), the vast majority had compound eyes. The most common trilobite eye was the holochroal type (Lindström 1901; Clarkson 1979), characterized by a large number of lenses (up to several thousand) covered by a single cuticular cornea. The schizochroal eye (Lindström 1901), with fewer and much larger lenses separated

[1] Address correspondence to Scott A. Lee, Department of Physics and Astronomy, University of Toledo, 2801 West Bancroft Street, Toledo, OH 43606, USA.
Email: Scott.Lee@utoledo.edu

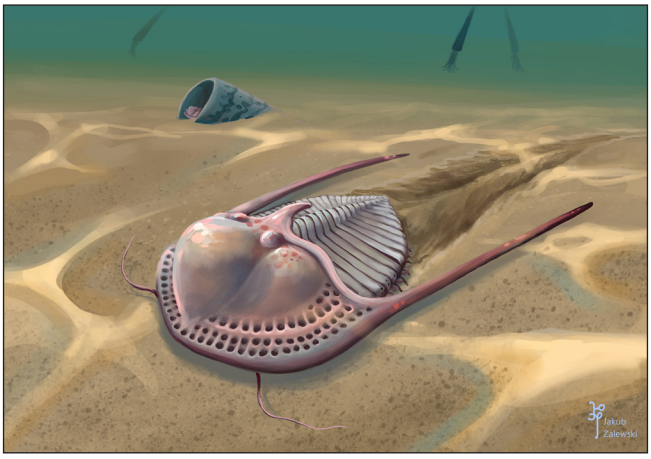

FIGURE 1. The blind *Cryptolithos* moving along the sea floor. Art by Jakub Zalewski (Warsaw, Poland) and used with permission.

by cuticular material, developed within only 1 family, the Phacopina (see Fig. 2 for an example). A third type, the abathochroal eye (Jell 1975) has been noted only in the small Cambrian eodiscids. This eye had small, less ordered lenses which were clearly separated from each other and each covered by a thin cornea.

In all 3 trilobite eye types, the focusing elements of trilobite eyes were calcite crystals (Clarkson et al. 2006). The very high refractive indices of calcite are 1.486 and 1.658 for the extraordinary and ordinary rays, respectively, at 590 nm (Bragg 1924). The structure of the calcite crystal in trilobite eyes was such that the light rays experience the ordinary index of refraction (Horvath 1989). This is a great advantage for a marine creature since the light rays can be brought to a focus at a short distance. This is superior to the chitin focusing component found in the eyes of all the other arthropods since the refractive index of chitin is 1.56 when dry and lower when hydrated (Horvath 1989). The birefringence of calcite could lead to double images, but the optic axis of the calcite in trilobite eyes was always normal to the visual surface (Horvath 1989). Consequently, normally-incident light that entered the eye experienced the ordinary index of refraction. For more information, an interested reader can refer to a number of studies that have characterized trilobite vision (Horvath 1989; Fordyce and Cronin 1993; Schoenemann et al. 2015, 2021; Schoenemann 2021). Trilobites eyes had a very large depth-of-field, which has inspired modern optical devices with similar properties (Fan et al. 2022).

Eyes allow an animal to perceive its environment by focusing light from objects in its surroundings onto its light-detecting apparatus. A cone of light rays from an object point is focused by the lens (and cornea) to form an image point, which contributes information about the object. This focusing effect causes the light within the cone to travel in specific directions. Any light not contributing to the foci on the light-detecting apparatus can arise from an object source when the ray from that source follows a path different from that intended, or more often, it can arise from a different source (Coleman 1947; Lytle and Morrow 1977).

Calcite is the stable polymorph of $CaCO_3$ under ambient conditions. With a band gap of 6.0 ± 0.4 eV (electron volts) (Baer and Blanchard 1993), calcite is transparent in the visible spectral range. Naturally occurring (both biogenic and geogenic) calcite crystals display photoluminescence (PL) from 400 to 700 nm when illuminated by ultraviolet (UV) light. When a UV-A photon—corresponding to a wavelength within the range 300 to 400 nm and a photon energy in the range 3.1 eV to 4.1 eV—is absorbed, an electron can be elevated from an initial state in the filled valence band to a second empty defect state within the bandgap having an energy above the initial state equal to that of the absorbed UV-A photon. Alternatively, the photon can excite an electron from a filled defect state to the empty conduction band. In either circumstance, this excited electron emits a number of phonons (quantized lattice vibrations), losing sufficient energy until it reaches a third state within the band gap of the calcite, which serves as the initial state of the PL transition. After a lifetime in the range of tens of nanoseconds to milliseconds, depending on the nature of the defect and the radiative rate, the electron transitions to an empty state generated by the initial excitation and emits a photon in the visible range (Gaft et al. 2008, 2015). Because of the energy distribution of defect or conduction band states associated with the excitation process, a range of UV wavelengths can excite PL in the sample. The current study considers the PL induced by UV-A wavelengths from 300 nm to 400 nm and its effect on the trilobite's vision.

States within the bandgap associated with both intrinsic and extrinsic defects can exist in calcite. Intrinsic defects include point, linear, and planar defects with their accompanying lattice distortions, examples being vacancies and interstitials, dislocations, and stacking faults, respectively. Extrinsic defects include impurities that can be substitutional or interstitial, together with their distortions. In calcite, the PL centers can be impurity ions (such as Mn^{2+}) substituting for Ca^{2+} ions, other chemical impurities (including organic matter), oxygen vacancies, and lattice imperfections and distortions (including dislocations of the CO_3^{2-} anion group) (Toffolo et al. 2019).

The calcite components of the eyes of trilobites are very rarely present in recovered fossilized specimens (Schoenemann et al. 2015). Also, chemical modifications of the calcite during the long burial for at least 250 million years could have changed the calcite crystals in unknown ways. Consequently, the nature of the PL process and the identity and concentration of the PL centers in the calcite of trilobites during their lifetime are both unknown. Extant red algae produce calcite crystals containing organic carbon 1.6% by weight and 54 ppm of Mn^{2+}, as shown by Pedone et al. (1990). These authors provided strong evidence that the associated residual organic matter is responsible for

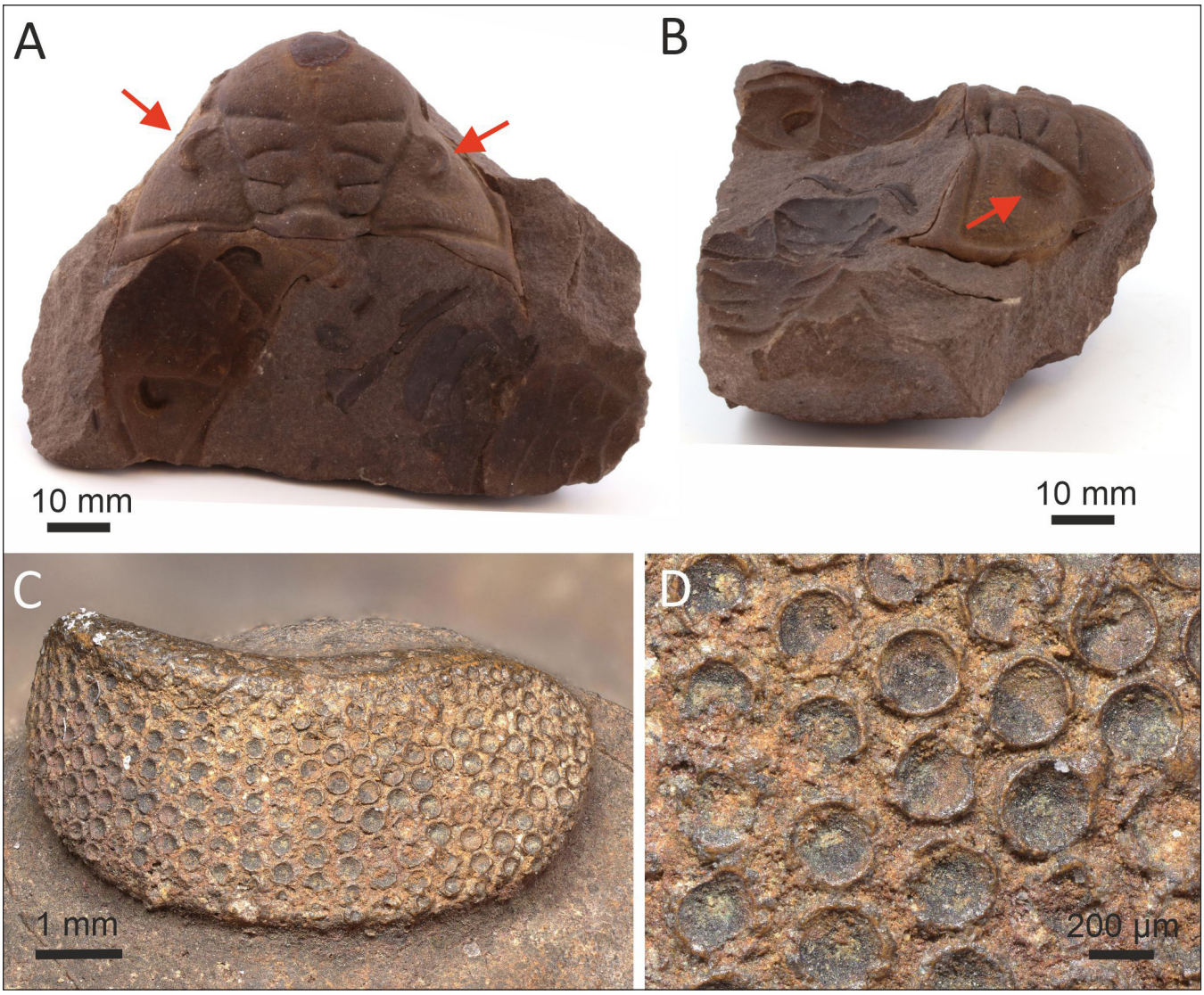

FIGURE 2. The cranidium (head) of the Upper Ordovician phacopid trilobite *Dalmanitina socialis* from Hostra Gora in the Prague Basin, Czech Republic, in dorsal (A) and side (B) views with eyes indicated by red arrows, a close-up of the right eye (C), and a close-up of the individual ommatidia (D). Specimen MWGUW 002541 on display in the Stanisław Józef Thugutt Museum of the Faculty of Geology, University of Warsaw, Poland. Photographs made by Mariusz Niechwedowicz (University of Warsaw) and used with permission.

the PL centers observed within this form of biogenic calcite. The organic matter is assumed to be cellular components incorporated into the calcite crystals during their growth. Since both trilobites and red algae are marine organisms, it is assumed that they incorporated this organic matter within their calcite in similar manners. Because the spectral shape of the PL provides a signature of the PL centers, it is also assumed that the spectral shape from red algae calcite is the same as that from trilobites. Note that the typical plant (such as red algae) cell is 10 to 100 μm in diameter while the typical animal (such as a trilobite) cell is about 10 to 20 μm in diameter. This difference in cell size might have created a density of PL centers in trilobites different from that in red algae. In addition (because the magnitude of the PL signal is proportional to the concentration of PL centers in the crystal) this concentration in red algae and trilobites were, most likely, not identical; however, their values are assumed to be within an order of magnitude of each other. Without an understanding of the nature of the PL excitations and PL transitions, as well as an accurate measurement of the concentration of PL centers in trilobite calcite, the magnitude of its PL is unknown.

The trilobite species *Dalmanitina socialis* (specimen MWGUW 002541 at Stanisław Józef Thugutt Museum of the Faculty of Geology, University of Warsaw, Poland), a member of the order Phacopida, is considered in the current study. UV-A sunlight penetrated some distance down into the Paleozoic seas and excited PL in the calcite crystals of the trilobite eyes, since biogenic calcite displays photoluminescence when exposed to UV-A radiation. In the current study, the PL light excited by the UV-A band is assumed to have the same characteristics as that observed by Pedone et al. (1990) using 363 nm UV radiation. This PL was emitted in all directions, some of which reached the photoreceptors of the trilobite eyes. For the PL light to be detected by the eye, the propagation vector of the light had to include a component directed toward the photoreceptors of the eye. Only half of the emitted PL light was emitted with such a component. A fraction of the light emitted with the appropriate component would have been lost, however, since it would have left the calcite crystal if it struck the side of the crystal at an angle less than the critical angle for total internal reflection—which is lower for the ordinary waves. Note that two-thirds of the emitted PL would have consisted of ordinary waves, having experienced the ordinary index of refraction, and one-third extraordinary, depending on whether these waves exhibited polarization components perpendicular and parallel to the optic axis, respectively. Consequently, less than half of the emitted PL light would have been detected by the trilobite's eye. Since this PL light conforms to the definition of stray light—not having arisen from an object being imaged—it would have lowered the contrast of the trilobite's vision, thereby obscuring its vision. Trilobites and brittle stars are the only known species in nature that had or have components that generate obscuring light in this way (Whitfield 2001).

The PL stray light (or obscuration, as described here) would have been similar to that generated by fog or haze, which scatters the original photons of light from an object being imaged. The photons are scattered into new directions unrelated to their original propagation, no longer carry information about their origin, and diminish the observed contrast. This effect of fog is usually quantified as an extinction coefficient γ, the propagation distance for a collimated beam of 550 nm light to be attenuated to a certain fraction (usually 5% or 2%) of its original irradiance (Grabner and Kvicera 2011). By comparison, the PL of calcite creates new photons by the absorption of the UV-A photons of light being imaged by the visual system. Each PL photon is emitted in an arbitrary direction and contains no information about the absorbed UV-A photon from the object. The PL photons in the visible range constitute stray light for the visual signal, since they contain no information about the original object.

Since eyes detect light by counting the number of photons arriving per unit time, the current study will calculate the rate at which visible photons are detected by the eye. There must have been 2 kinds of visible photons in the trilobite's eyes: the visible sunlight photons that originated in the photosphere of the Sun, referred to here as *solar photons*, and the visible photons created by PL in the calcite, referred to here as *PL photons*.

This unique system of vision relying on calcite lenses requires, in turn, a unique parameter to quantify the obscuration effect generated by the

stray light. This parameter is defined here for the first time and called the *obscuration factor* φ and defined to be the total number of PL photons seen by the trilobite per second, $\dot{N}_{eye,tot}^{PL}$, divided by the total number of the visible solar photons seen by the trilobite per second, $\dot{N}_{eye,tot}^{solar}$.

$$\varphi = \frac{\dot{N}_{eye,tot}^{PL}}{\dot{N}_{eye,tot}^{solar}} \qquad (1)$$

The dot over a symbol signifies its time derivative. The quantities in both the numerator and denominator have been summed over the entire visible spectrum. If there were no PL, the obscuration factor φ would be 0, and the trilobite would see with maximum contrast. The presence of any photoluminescence in the calcite meant that the obscuration factor was greater than 0. As the amount of PL increased, the obscuration factor increased, and the contrast of the trilobite's vision decreased.

This paper presents, for the first time, a quantitative evaluation of the effects of PL on the vision of trilobites. These calculations directly address the suggestion by Schoenemann et al. (2015) that the obscuring effect of PL in the trilobite vision should decrease with ocean depth. A number of specialized terms from optics are used in these theoretical calculations and a glossary (Table 1) is given for the reader's convenience.

Table 1
Definitions of physical parameters used in these calculations

Parameter	Definition
$\varphi(d)$	Total rate of PL photons detected by eye at depth d divided by the total rate of solar photons detected by eye at depth d
$\dot{N}_{eye,tot}^{PL}(d)$	Total rate of PL photons detected by eye at depth d
$\dot{N}_{eye,tot}^{solar}(d)$	Total rate of solar photons detected by eye at depth d
$\dot{N}_{eye}^{PL}(\lambda,d)$	Rate of PL photons of wavelength λ per unit wavelength detected by eye at depth d
$\dot{N}_{eye}^{solar}(\lambda,d)$	Rate of solar photons of wavelength λ per unit wavelength detected by eye at depth d
$\dot{N}^{PL}(\lambda,d)$	Rate at which PL photons of wavelength λ per unit wavelength are created at depth d
$\dot{N}^{solar}(\lambda,d)$	Rate at which solar photons of wavelength λ per unit wavelength arrive at depth d
$P_{tot}^{UV-A}(d)$	Total power of solar UV-A radiation with wavelengths between 300 and 400 nm at depth d inside the calcite crystal
$P^{UV-A}(\lambda,d)$	Power of solar UV-A radiation of wavelength λ per unit wavelength at depth d inside the calcite crystal
$(Irr)^{UV-A}(\lambda,d)$	Irradiance of solar UV-A radiation of wavelength λ per unit wavelength at depth d
$P^{solar}(\lambda,d)$	Power of solar visible light of wavelength λ per unit wavelength arriving at depth d
$(Irr)^{solar}(\lambda,d)$	Irradiance of solar visible light of wavelength λ per unit wavelength arriving at depth d
$F^{PL}(\lambda)$	Spectral profile of photoluminescence photons of wavelength λ per unit wavelength created by solar UV-A radiation
$R_{sur}(\lambda)$	Reflectance of a surface as a function of wavelength λ
$T_{int}(\lambda)$	Transmittance of the water-calcite interface as a function of wavelength λ
$S_{sye}(\lambda)$	Probability that a photon of wavelength λ will be detected by eye

For biogenic calcite, PL data were measured by laser excitation at the single UV-A wavelength of 363 nm (Pedone et al. 1990). As will be detailed later, their work implied that the PL happens only very rarely in red algae calcite: the probability that PL will occur for a particular UV photon incident on a particular PL center is about 3×10^{-8}. This raises the possibility that the number of PL photons per second present in the vision of trilobites was smaller (and perhaps much smaller) than the noise in the number of solar photons per second, meaning that the trilobite would not have been able to detect such PL light. However, a direct calculation of the PL photon count rate for trilobites $\dot{N}_{eye,tot}^{PL}$ requires an understanding of the nature of the PL process and determination of the number density of the defect states in their calcite.

A calculation is performed assuming that trilobites had the same type and number density of PL centers as red algae calcite. A second set of calculations is performed which eliminated all unknown parameters (including, for example, the concentration of the PL centers) to calculate how φ changes with depth but not the absolute value of φ at any depth. Depths of 1 cm, 1 m, and 10 m are chosen for the current calculations since Schoenemann et al. (2015) carefully determined the incident visible solar radiation at those 3 depths below the ocean's surface. The size and shape of the object and the relative positioning of the trilobite, the object, and the Sun are kept the same for all 3 depths. This work provides clear evidence that the obscuration effect of PL in the eyes of trilobites decreased with depth, as originally suggested by Schoenemann et al. (2015). No significant obscuration was present at a depth of 10 m in the Paleozoic seas; that is, no significant PL photon count rate is calculated at a depth of 10 m.

Two different objects are considered for the second set of calculations: 1) a white object, assumed to have the same ultraviolet and visible reflectance of a white pearl reported in the 0/d observational geometry (Karampelas et al. 2011); and 2) a brown object, assumed to have the same reflectance as brown printed fabric reported in the d/0 geometry (Jafari et al. 2016). The latter diffusely-incident and normally-reflected d/0 configuration is more relevant for the visual configuration of the trilobite eye. Thus, for an appropriate comparison, it is assumed that the reflectance of white pearl in the normally-incident diffusely-reflected 0/d configuration is the same as that in the d/0 configuration (Budde 1976). Pearl is composed of 95% aragonite, a crystalline form of $CaCO_3$, and 5% conchiolin, a scleroprotein (Agatonovic-Kustrin and Morton 2012). The white object is expected to be seen more easily due to its higher d/0 reflectance compared to the brown object, which is also more effectively camouflaged in the marine environment.

The visual range is assumed to be from 400 to 700 nm, the same as in the extant marine crustacean *Squilla empusa*, a distant living relative of the trilobites (Cronin 1985). Although the reflectance of the objects for incident diffuse light has been specified, the exact amount of scattered and reflected sunlight entering the eye is unknown since the current authors have not specified the visual system geometry relative to the source and object. Only a certain fraction of scattered and reflected sunlight will enter the eye from the object. Since the geometry of the system is held constant at each depth, the same fraction of sunlight will enter the eye at each depth. By dividing the obscuration factor at 1 m and 10 m by its value at 1 cm, the unknown fraction is eliminated and the effect of depth on the obscuration factor is determined. As originally suggested by Schoenemann et al. (2015), the scaled obscuration factor observed by the trilobite is expected to decrease with increasing depth.

As shown in Equation (1), the obscuration factor is defined to be the rate at which PL light is detected by the eye divided by the rate at which sunlight reflected and scattered by the object is detected by the eye. Note that both quantities are represented by summations of the corresponding spectral quantities over all wavelengths of the visual range. Except for the calculation of the magnitude of the PL light compared to the photon noise in the solar light, the general approach is the following.

First, the denominator of Equation (1), the rate at which solar photons at depth d, $\dot{N}_{eye,tot}^{solar}(d)$, were detected by the eye is evaluated. Note that water waves on the ocean's surface will generate converging light rays over certain regions of the sea floor and diverging rays in other regions, as illustrated in Fig. 1. Over time, these effects average to zero and the average current solar spectral irradiance is used for the calculations. The rate at which solar photons were detected at depth d, $\dot{N}_{eye,tot}^{solar}(d)$, is determined by summing the rate at which solar photons within

each narrow wavelength band Δλ about λ were detected at depth d, $\dot{N}_{eye}^{solar}(\lambda,d)\Delta\lambda$, spanning all visible wavelengths (400 to 700 nm). The spectral rate of solar photons of wavelength λ detected by the eye, $\dot{N}_{eye}^{solar}(\lambda,d)$, is proportional to the spectral rate $\dot{N}^{solar}(\lambda,d)$ at which solar photons of wavelength λ reach the depth d, the reflectance, $R_{sur}(\lambda)$, of the surface of the imaged object for the incident light, the normal incidence transmittance $T_{int}(\lambda)$ of the water-calcite interface, and the probability, $S_{eye}(\lambda)$, that the photon will be absorbed and detected by the visual system. It can be assumed that $R_{sur}(\lambda)$ is applicable irrespective of the nature of the incident light on the object, whether it is directed at a specific angle of incidence or diffused at all angles. The transmittance $T_{int}(\lambda)$ is not unity due to the different refractive indices of water and calcite. It is assumed that the probability $S_{eye}(\lambda)$ in trilobites was the same as in *Squilla empusa* (Cronin 1985).

Since sea water transmits light in the blue and green region of the spectrum more effectively than at longer wavelengths, it is expected that eyes operating in the marine environment were most sensitive in the blue and green portion of the visible spectrum, as observed in *S. empusa*. The spectral rate at which solar photons of wavelength λ arrive at depth d, $\dot{N}^{solar}(\lambda,d)$, is related to the spectral power of the visible light, $P^{solar}(\lambda,d)$, at that depth via the energy of each photon,

$$\dot{N}^{solar}(\lambda, d) = \frac{P^{solar}(\lambda,d)}{hc/\lambda},$$

where h is Planck's constant and c is the speed of light. The power is related to the spectral irradiance of the solar photons at depth d with wavelength λ:

$$(Irr)^{solar}(\lambda, d) = P^{solar}(\lambda, d)/A,$$

where A is the area over which the solar power is measured. The irradiance is a measured quantity given in Schoenemann et al. (2015) for the depths under consideration. This permits the evaluation of the denominator of Equation (1) to within a single constant.

Second, the numerator of Equation (1), $\dot{N}_{eye,tot}^{PL}(d)$, the rate at which the total PL photons are detected by the eye at ocean depth d is evaluated. This rate is determined by summing the rate at which PL photons within each wavelength band Δλ centered at λ and at depth d are detected by the eye, $\dot{N}_{eye}^{PL}(\lambda,d)\Delta\lambda$, over all wavelengths in the visual range. $\dot{N}_{eye}^{PL}(\lambda,d)$ is proportional to the spectral rate that the PL photons of wavelength λ are created in the trilobite's eye at depth d. The nature and number density of PL sites in the calcite is unknown, introducing an unknown constant into the calculations describing the PL efficiency. The PL photons will be emitted in all directions. An unknown fraction of the emitted PL photons will arrive at the light-detecting apparatus, introducing a second unknown parameter. However, these 2 parameters multiply each other, resulting in a single unknown parameter. The rate $\dot{N}_{eye}^{PL}(\lambda,d)$ is also proportional to the sensitivity of the photoreceptor at the PL wavelength, $S_{eye}(\lambda)$. The visible PL photon creation rate is proportional to the total power of the UV-A band, $P_{tot}^{UV-A}(d)$, inside the eye after accounting for the normal incidence transmittance $T_{int}(\lambda)$ of the calcite-water interface in the UV-A range. The creation rate is also proportional to the spectral efficiency at which the PL is generated from those UV photons, $F^{PL}(\lambda)$, given in units of counts per second per mW excitation per nm wavelength. It is assumed that $F^{PL}(\lambda)$ for the calcite in trilobites is the same as for modern red algae measured by Pedone et al. (1990).

The total power of the UV-A band, $P_{tot}^{UV-A}(d)$, at various depths is determined by summing the power of the UV-A band within the wavelength band Δλ centered at λ, $P^{UV-A}(\lambda,d)\Delta\lambda$, over all UV-A wavelengths. Here $P^{UV-A}(\lambda,d)$ is the spectral UV power at wavelength λ and depth d, from 300 to 400 nm. It is necessary to account for the reflectance of the white or brown object, which is approximated to be independent of the nature of the incident light.

The UV-A content of solar radiation incident on the Earth's surface depends on both the output of the Sun and the composition of the atmosphere. Models of stellar evolution show that the temperature of the Sun's photosphere throughout the Paleozoic Era differed from the current Sun by less than 0.02% (Ribas 2009). Since the oxygen content of the atmosphere fluctuated throughout the Paleozoic Era, the results of the current study are only valid for the times that the ancient atmosphere had the same content as the current atmosphere. Thus, $P^{UV-A}(\lambda,d)$ is determined by using the known irradiance of UV-A radiation at the same wavelength at the surface of the modern ocean. This irradiance is given in the ASTM G173-03 Reference Spectra derived from SMARTS v. 2.9.2, published by the National

Renewable Energy Laboratory (NREL 2023). The refractive indices of sea water are used to calculate the fraction of UV-A radiation that was reflected by the ocean's surface. Measurements of the absorption of UV-A radiation (Armstrong and Boalch 1961) then allowed for the calculation of the UV-A irradiance as a function of depth, $(Irr)^{UV-A}(\lambda,d)$. This permits the evaluation of the numerator of Equation (1) to within a single constant.

Dividing the numerator by the denominator permits evaluation of the obscuration factor φ to within a constant at the 3 depths under investigation (1 cm, 1 m, and 10 m). Dividing the obscuration factors at 1 m and 10 m by the result at 1 cm, then yields a parameter-free result for the scaled obscuration factor which allows for an evaluation of the hypothesis. This reveals the change of the obscuration factor with depth.

METHODS AND MATERIALS

Pedone et al. (1990) measured the PL profile $F^{PL}(\lambda)\Delta\lambda$, of PL light emitted by red algae calcite when excited by 363 nm UV-A radiation from an Ar^+-ion laser, as shown in Fig. 3. They excited this spectrum by illuminating the sample with 1 mW of laser power and measured it with a spectral resolution of $\Delta\lambda = 0.1$ nm. The observed PL under these conditions has the same photon count rate as shown along the y-axis of Fig. 3 after multiplication by 1 mW.

Dividing those count rates by the spectral resolution $\Delta\lambda$ gives $F^{PL}(\lambda)$, the spectral count rate in counts/(s·mW·nm), and integrating that gives the total PL photon count rate. Pedone et al. (1990) states that these data were taken with a microscope objective having a numerical aperture of 0.85. Therefore, their apparatus collected PL photons emitted within a solid angle of 0.946 π steradians, and the total PL photon count rate needs to be multiplied by the geometrical factor of 4 π/0.946 π (= 4.2) to determine the total PL count rate for all directions. This calculation will help to determine the efficiency with which PL photons are created by incident UV photons.

The calculations in the current study are based on a model of the vision of a trilobite whose calcite displays the same kind of PL as extant red algae and with the assumption that the probability of its eye detecting a photon of wavelength λ is the same as in the extant marine crustacean *Squilla empusa*.

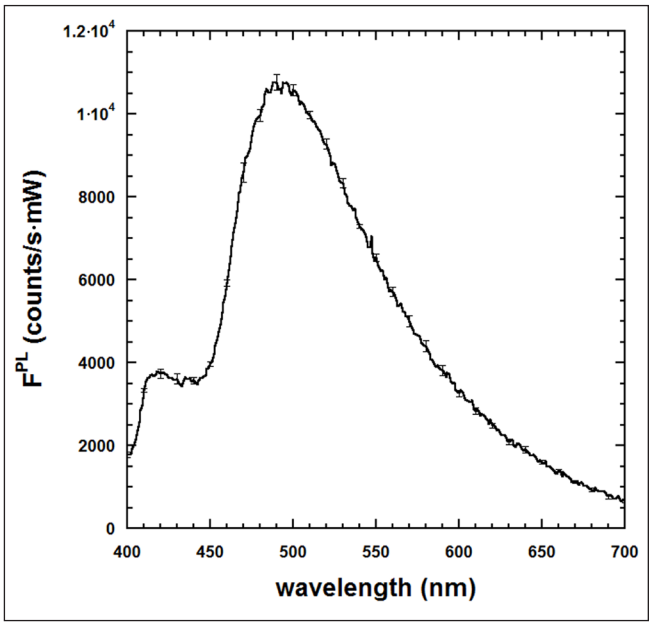

FIGURE 3. The photoluminescence profile $F^{PL}(\lambda)\Delta\lambda$, measured in counts/(s·mW), as a function of wavelength, measured in nm, when excited by 1 mW of 363 nm UV-A radiation from an Ar^+-ion laser. $F^{PL}(\lambda)\Delta\lambda$ was measured with a spectral resolution of Δλ = 0.1 nm and a numerical aperture of 0.85 for the collection optics. Data are from Pedone et al. (1990). The error bars are 1 standard deviation. For clarity, only every 10th error bar is shown.

The following methodology is used in this study's full calculations of the visual system of a trilobite. It is assumed that all eyes have a wavelength-dependent probability, $S_{eye}(\lambda)$, that a photon of wavelength λ will be detected. It is further assumed that 1) the probability of photon detection is the same as the probability of photon absorption and 2) the probability of absorption in trilobites was the same as in the extant *Squilla empusa* (Cronin 1985), as stated earlier, and shown in Fig. 4. Note that the visual range for *S. empusa* is from 400 to 700 nm.

Recall that Equation (1) yields the obscuration factor for the trilobite's vision. The very compact form of this equation must be expanded in terms of measured quantities for its evaluation. Note that the denominator of Equation (1) is given by

$$\dot{N}^{solar}_{eye,tot}(d) = \sum_{\lambda=400}^{700} \dot{N}^{solar}_{eye}(\lambda, d)\,\Delta\lambda, \qquad (2)$$

where $\dot{N}^{solar}_{eye}(\lambda,d)$ is the spectral rate at which solar photons of wavelength λ were detected by the trilobite's eye at ocean depth d. This rate has units of counts per second per nm wavelength and Δλ is the wavelength increment, which is taken to be 1 nm by selecting 301 wavelength points from 400 nm to 700 nm. $\dot{N}^{solar}_{eye}(\lambda,d)$ is proportional to the rate at which the solar photons were available to enter

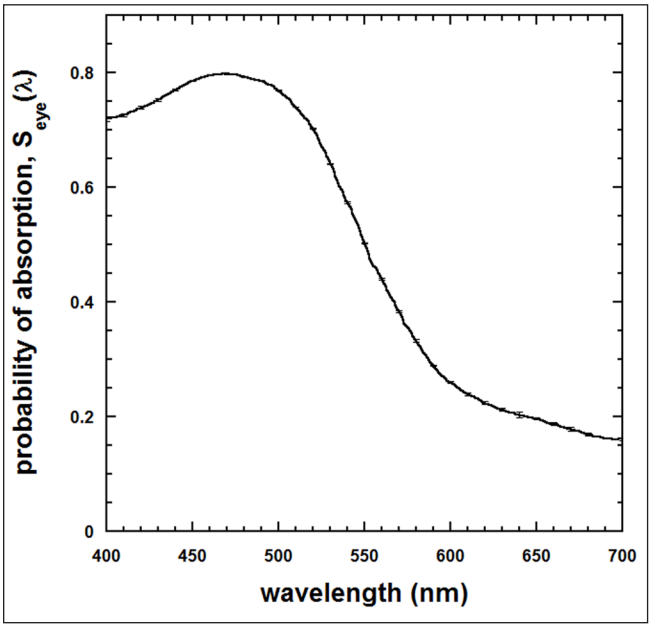

FIGURE 4. The sensitivity $S_{eye}(\lambda)$ (the probability of photon absorption) of the photoreceptors in the compound eyes of the extant marine crustacean *Squilla empusa* as a function of wavelength (in nm). The data are from Cronin (1985). The error bars show 1 standard deviation. Only every tenth error bar is shown for clarity. The error bars are very small on the scale of $S_{eye}(\lambda)$.

the trilobite's eye. It is also proportional to the transmittance of the water-calcite interface and to the sensitivity of the photoreceptor at wavelength λ (taken as the probability of absorption in Fig. 4). This rate further depends on the geometry of the relative positions of the imaged object and the trilobite's eye (which are the same at all ocean depths). Therefore, $\dot{N}_{eye}^{solar}(\lambda,d)$ is given by

$$\dot{N}_{eye}^{solar}(\lambda,d) = \alpha\, T_{int}(\lambda) S_{eye}(\lambda)\, \dot{N}^{solar}(\lambda,d), \quad (3)$$

where $\dot{N}^{solar}(\lambda,d)$ is the spectral rate at which solar photons of wavelength λ arrived at depth d after interaction with the object being imaged by the visual system, $T_{int}(\lambda)$ is the transmittance of the water-calcite interface with assumed normal incidence, $S_{eye}(\lambda)$ is the sensitivity of the photoreceptor, and α is a constant. The value of α is unknown but determined by the geometry of detection relative to the object, involving: the distance between the object and the trilobite's eye, the angle between the normal of the object surface being imaged and the normal of the eye's surface (along which the detected rays enter), the numerical aperture of the eye, and the eye's internal optics—including the reflectance and scattering by the interface between the calcite and the light-detecting apparatus.

The spectral rate at which solar photons of wavelength λ arrived at depth d, $\dot{N}^{solar}(\lambda,d)$, is determined by the spectral power of the solar photons with wavelength λ and the energy of each photon:

$$\dot{N}^{solar}(\lambda,d) = \frac{P^{solar}(\lambda,d)}{hc/\lambda}\,. \quad (4)$$

The spectral power of the solar photons with wavelength λ at depth d arriving at the eye is given by

$$P^{solar}(\lambda,d) = R_{sur}(\lambda) \times (Irr)^{solar}(\lambda,d) \times A\,, \quad (5)$$

where $R_{sur}(\lambda)$ is the reflectance at wavelength λ of the object's surface assumed to be obtained in the d/0 configuration, $(Irr)^{solar}(\lambda,d)$ is the spectral irradiance of the solar photons with wavelength λ at depth d, and A is the cross-sectional area of the calcite crystal. The cross-sectional area of the ommatidia of the eye of the trilobite *Dalmanitina socialis* is used in these calculations, determined from Fig. 2, to be (6.24 ± 0.69) × 10^{-8} m^2 (mean and standard deviation). Both $P^{solar}(\lambda,d)$ and $(Irr)^{solar}(\lambda,d)$ in Equation (5) are spectral quantities measured in units of W/(m^2·nm) with the latter shown in Fig. 5. Schoenemann et al. (2015) used the results of Wozniak and Dera (2007) to construct the solar spectral irradiance from 400 to 2,500 nm at depths of 1 cm, 1 m, 10 m, and 100 m in sea seawater. The spectral irradiance of UV-A radiation at a depth of 100 m in the ocean is sufficiently small so that no calculations are performed for that depth in the current work.

Combining Equations (2) through (5), the following expression is obtained:

$$\dot{N}_{eye,tot}^{solar}(d) = \alpha \sum_{\lambda=400}^{700} \frac{\lambda\, T_{int}(\lambda) S_{eye}(\lambda) R_{sur}(\lambda)\, (Irr)^{solar}(\lambda,d) \times A \times \Delta\lambda}{hc} \quad (6)$$

The reflectance spectra $R_{sur}(\lambda)$ for both the white and brown objects are given in Fig. 6, based on an assumption of the d/0 optical configuration and a measurement in that configuration, respectively. In such a configuration, it is reasonable to propose that $R_{sur}(\lambda)$ is independent of the nature of the light incident on the object, whether diffuse or direct. Differences between the geometry of the detection system for the $R_{sur}(\lambda)$ measurements, and that of the trilobite's eye, are taken into account by the parameter α.

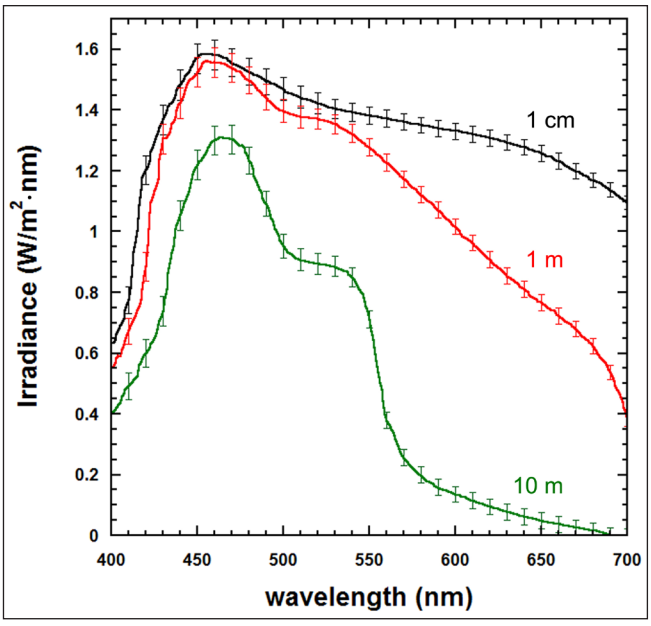

FIGURE 5. The spectral irradiance (in W/m²·nm) as a function of wavelength (in nm) for solar visible light at depths of 1 cm (black), 1 m (red), and 10 m (green) in seawater. The error bars are 1 standard deviation. For clarity, only every 10th error bar is shown. The data are from Schoenemann et al. (2015) and the error bars are from NREL (2023).

The probability that the eye absorbs a photon of wavelength λ, $S_{eye}(\lambda)$, is shown in Fig. 4. The transmittance for the water-calcite interface was calculated from the standard formula for the transmission of normal incidence light on an interface between 2 media with different refractive indices (Lepley and Adams 1968) and is shown in Fig. 7. The refractive indices versus wavelength for calcite and water are from Ghosh (1999) and Hale and Querry (1973), respectively. Recall that, due to the crystallographic orientation, the incident light experiences only the ordinary index of refraction in trilobites for the solar photons (Horvath 1989).

By performing the sum in Equation (6) over 301 terms from λ = 400 nm to 700 nm, the wavelength increment Δλ is set to 1 nm. Thus, the data from Figs. 4, 5, 6, and 7 allows evaluation of Equation (6); however, a value must be assigned to the unknown constant α.

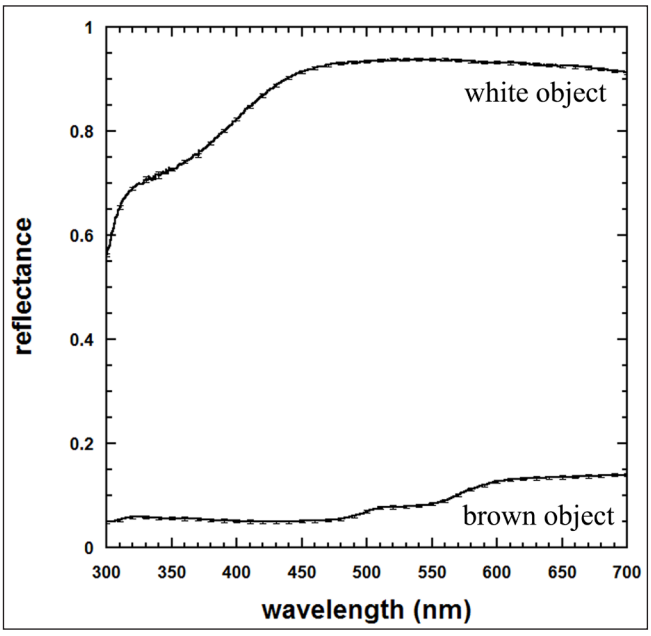

FIGURE 6. Reflectance as a function of wavelength for the white and brown objects from Karampelas et al. (2011) and Jafari et al. (2016), respectively. Every tenth error bar (equal to 1 standard deviation) is shown.

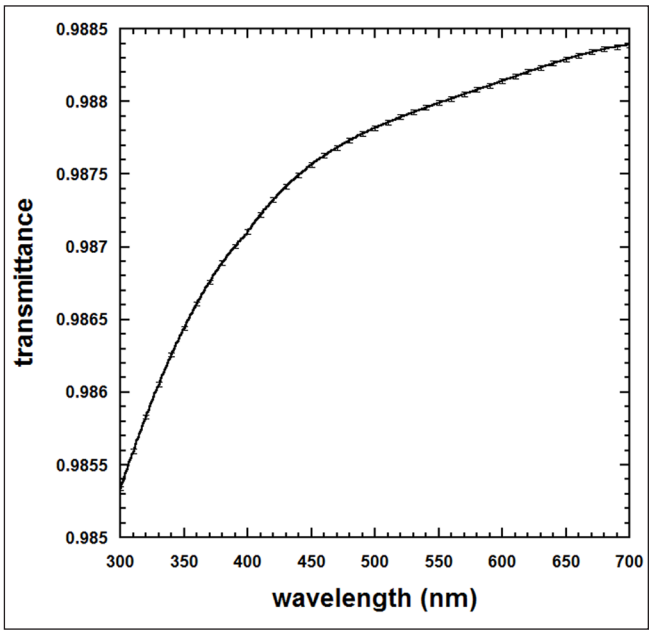

FIGURE 7. The transmittance for the water-calcite interface for normal incidence light. Every tenth error bar (equal to 1 standard deviation) is shown.

Next, attention is turned to the numerator of Equation (1):

$$\dot{N}^{PL}_{eye,tot}(d) = \sum_{\lambda=400}^{700} \dot{N}^{PL}_{eye}(\lambda, d)\, \Delta\lambda, \quad (7)$$

where $\dot{N}^{PL}_{eye}(\lambda,d)$ is the spectral rate at which PL photons of wavelength λ were detected by the trilobite's eye at ocean depth d. The rate $\dot{N}^{PL}_{eye}(\lambda,d)$ is proportional to the rate that the PL photons of wavelength λ were created in the trilobite's eye at depth d and to the sensitivity of the photoreceptor at wavelength λ (shown in Fig. 4). Therefore, $\dot{N}^{PL}_{eye}(\lambda,d)$ is given by

$$\dot{N}^{PL}_{eye}(\lambda, d) = \beta_1\, S_{eye}(\lambda)\dot{N}^{PL}(\lambda, d), \quad (8)$$

where β_1 is the constant of proportionality determined by the fraction of PL photons which entered the photoreceptor and $\dot{N}^{PL}(\lambda,d)$ is the rate at which PL photons of wavelength λ were created in the calcite at ocean depth d.

The photoluminescence was created by the UV-A radiation in the incident sunlight. In order to calculate $\dot{N}^{PL}(\lambda,d)$, the total power of the UV-A radiation at the various depths, $P^{UV-A}_{tot}(d)$, must be determined. The transmittance of the UV-A radiation into the calcite from the water, $T_{int}(\lambda)$, must be calculated, however, to determine the UV-A power inside the calcite. The efficiency with which UV-A radiation was converted into visible PL photons of wavelength λ will be assumed to have the same spectral shape as for red algae calcite, shown in Fig. 3 (Pedone et al. 1990). A constant β_2 accounts for the conversion efficiency of the PL, which in turn depends on the number density and radiative rates of the PL centers in the trilobite eyes, as well as the effective numerical aperture of the trilobite's eye relative to that in the experiments of Pedone et al. (1990). This constant is almost certainly different than in red algae calcite and can be either larger or smaller than 1, depending on the relative concentrations and the radiative rates of the PL centers in trilobites and red algae. Since these centers are biogenic in origin, it is expected that their characteristics generate a β_1 value within the range of 0.1 to 10, though other values are possible. As a result of these considerations,

$$\dot{N}^{PL}(\lambda, d) = P^{UV-A}_{tot}(d) \times \beta_2 F^{PL}(\lambda). \quad (9)$$

The total power of the UV-A radiation inside the eye at the various ocean depths, $P^{UV-A}_{tot}(d)$, is given by

$$P^{UV-A}_{tot}(d) = \sum_{\lambda=300}^{400} T_{int}(\lambda) \times P^{UV-A}(\lambda, d)\, \Delta\lambda, \quad (10)$$

where $P^{UV-A}(\lambda,d)$ is the UV-A spectral power at wavelength λ inside the calcite crystal at depth d. It is determined by the UV-A irradiance $(Irr)^{UV-A}(\lambda,d)$ inside the calcite crystal, the reflectance $R_{sur}(\lambda)$ of the white or brown object at the same wavelength, the same constant α determined by the geometry of the object relative to the trilobite's eye (as discussed earlier), and the cross-sectional area A of the calcite crystal of the trilobite's eye:

$$P^{UV-A}(\lambda, d) = \alpha \times R_{sur}(\lambda) \times (Irr)^{UV-A}(\lambda, d) \times A\,. \quad (11)$$

The amount of UV-A radiation emitted by the Sun is determined by the temperature of its photosphere. No direct measurements of this temperature during the Paleozoic Era exist. However, theories of stellar evolution provide models that predict the temperature of the photosphere as a function of the Sun's age. Ribas (2009) reported that the temperature of the Sun's photosphere has undergone a very slight linear warming for the last 550 million years and is less than 0.2% warmer now than it was at the beginning of the Paleozoic Era. Consequently, the UV-A output of the Sun during the Paleozoic is assumed to be the same as today.

The amount of UV-A radiation which reaches the surface of the Earth is affected by Rayleigh multiple scattering and, below 350 nm, by the absorption onset of the ozone layer of the atmosphere (McClatchey et al. 1971). The latter is dependent on the amount of molecular oxygen in the atmosphere. The concentration of atmospheric oxygen has changed dramatically since the formation of the Earth. Constructing an accurate history of the composition of Earth's atmosphere is an active area of current research. During the Paleozoic Era, the amount of oxygen in the atmosphere is generally believed to have fluctuated between about 18% and about 25 to 30% (Krause et al. 2018; Brand et al. 2021;

Cooke et al. 2022). The amount of ozone in the atmosphere is determined by the Chapman cycle in which UV radiation cleaves molecular oxygen into 2 atoms of oxygen. The oxygen atoms can then combine with an oxygen molecule to form ozone. At times during the Paleozoic, the atmosphere would have had the same optical properties as it does today. The exact times of these congruencies are unclear due to differences in the results from the various atmospheric models. The calculations in the current study assume the same properties as today and, therefore, they are relevant only to times of the congruencies.

The ASTM G173-03 Reference Spectra derived from SMARTS v. 2.9.2, published by the National Renewable Energy Laboratory (NREL 2023), match the visible solar spectrum at the Earth's surface of Schoenemann et al. (2015). This reference's solar spectral irradiance in the UV-A band (300 to 400 nm) is used to determine the UV irradiance at the depths of 1 cm, 1 m, and 10 m. The normal incidence reflection coefficient for the air-water interface was calculated from the refractive indices of water and air in that range of wavelengths (Hale and Querry 1973) to determine how much UV-A radiation entered the seawater. Armstrong and Boalch (1961) measured the UV absorbance of seawater which is shown in Fig. 8 over the UV-A range.

These absorbance data were used to calculate the UV-A irradiances at depths of 1 cm, 1 m, and 10 m, which are shown in Fig. 9. The UV irradiance data of Fig. 9 and the object's reflectance of Fig. 6 are used in Equation (11) to calculate $P^{UV-A}(\lambda,d)$. The total UV-A power $P_{tot}^{UV-A}(d)$ is calculated via Equation (10) and the normal incidence transmittance of the water-calcite interface, shown in Fig. 7.

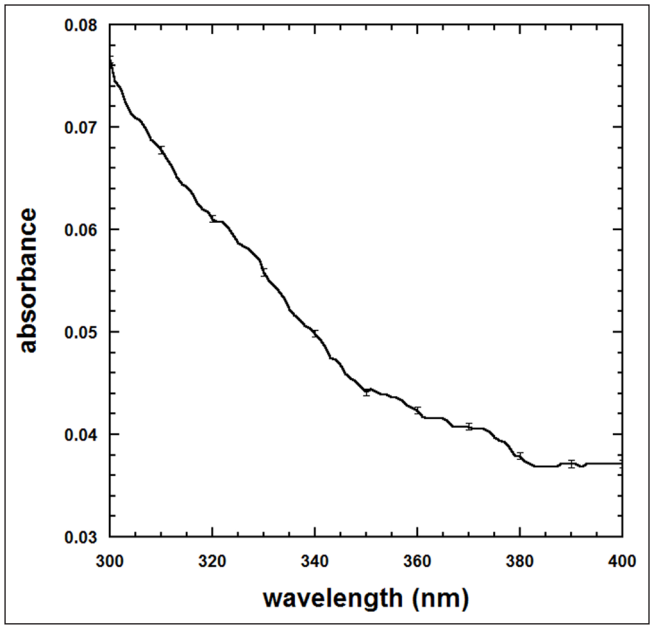

FIGURE 8. The UV absorbance of sea water in a 10 cm cuvette as a function of wavelength. The data are from Armstrong and Boalch (1961). Every tenth error bar (equal to 1 standard deviation) is shown for clarity.

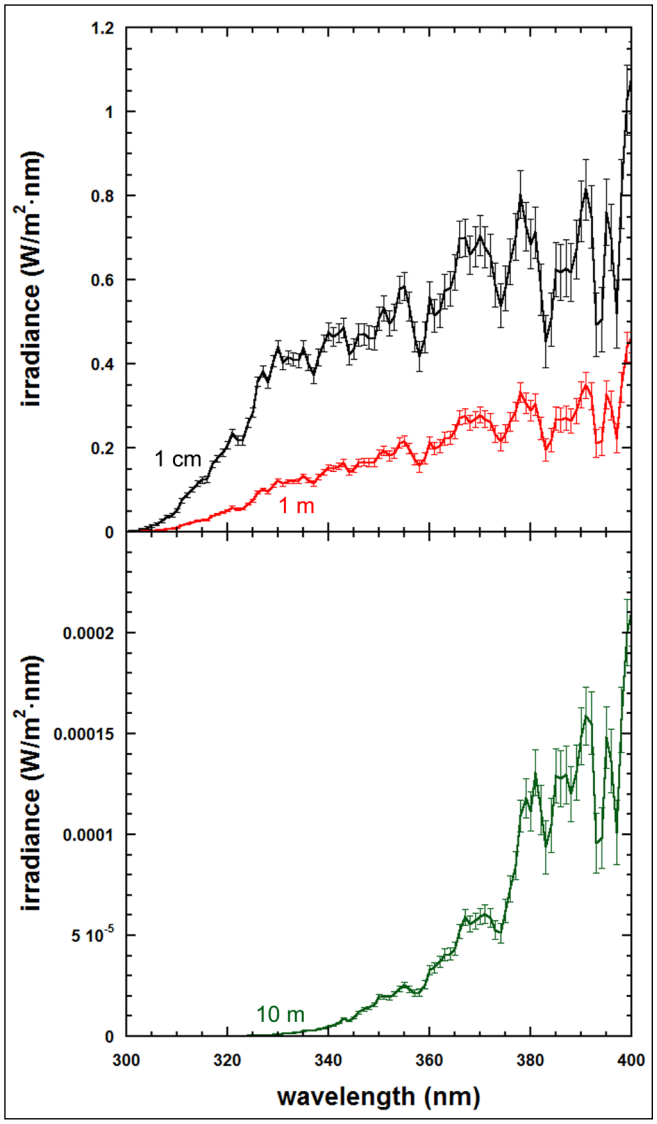

FIGURE 9. The UV-A spectral irradiance (in units of W/m^2 · nm) at depths of 1 cm (black), 1 m (red), and 10 m (green) as a function of wavelength (in nm) between 300 and 400 nm (the UV-A band). The error bars are 1 standard deviation. The data are from (NREL 2023) and modified appropriately for the normal incidence reflectance of the air-sea water interface and the UV-A absorbance of seawater.

$$\dot{N}_{eye,tot}^{PL}(d) = \alpha\beta \left(\sum_{\lambda=300}^{400} T_{int}(\lambda) R_{sur}(\lambda) \, (Irr)^{UV-A}(\lambda, d) \times A \times \Delta\lambda\right)\left(\sum_{\lambda=400}^{700} S_{eye}(\lambda) \, F^{PL}(\lambda)\Delta\lambda\right),$$

Equation (12).

$$\varphi(d) = \frac{\alpha\beta \left(\sum_{\lambda=300}^{400} T_{int}(\lambda) R_{sur}(\lambda) (Irr)^{UV-A}(\lambda,d)\times A\times\Delta\lambda\right)\left(\sum_{\lambda=400}^{700} S_{eye}(\lambda) \, F^{PL}(\lambda)\Delta\lambda\right)}{\alpha \sum_{\lambda=400}^{700} \frac{\lambda \, S_{eye}(\lambda) \, Irr^{solar}(\lambda,d) \times A \times \Delta\lambda}{hc}},$$

Equation (13).

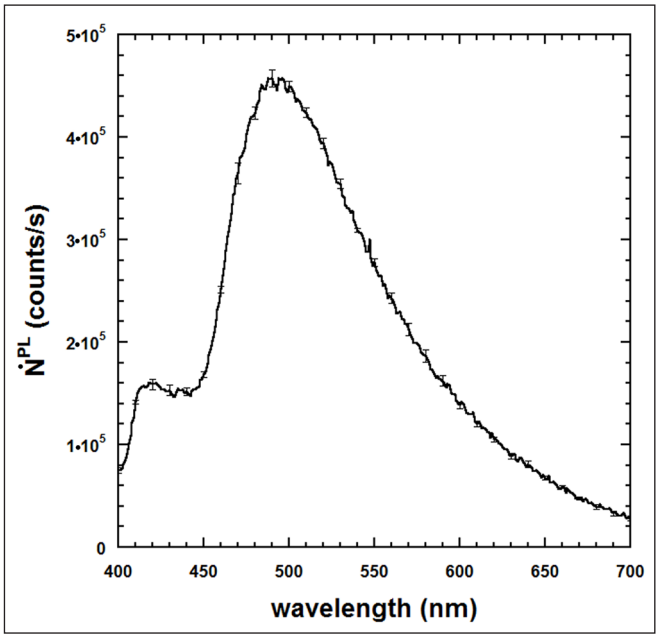

FIGURE 10. The count rate of the PL photons $\dot{N}^{PL}(\lambda)$ emitted in all directions by red algae calcite when excited by 1 mW of 363 nm UV-A radiation as a function of wavelength. The error bars show 1 standard deviation. Only every 10th error bar is shown for clarity.

Combining Equations (7) through (11) yields Equation (12) (shown above), where $\beta = \beta_1\beta_2$. Finally, Equations (1), (6), and (12) yield Equation (13) (shown above). All the quantities on the right-hand side of Equation (13), except for the parameters α and β, are known at the depths of 1 cm, 1 m, and 10 m. Note that α appears in both the numerator and denominator and therefore cancels out, leaving only the parameter β. Since the value of β is not known with certainty, the absolute value of $\varphi(d)$ cannot be determined. However, dividing both $\varphi(d = 1\text{ m})$ and $\varphi(d = 10\text{ m})$ by $\varphi(d = 1\text{ cm})$ yields how the scaled $\varphi(d)$ varied with depth since the unknown β cancels out:

$$\varphi_{scaled}(d) = \frac{\varphi(d)}{\varphi(0.01\text{ m})}. \qquad (14)$$

RESULTS

The efficiency of the PL process in red algae calcite is calculated by determining the number of visible PL photons emitted in all directions by the calcite when excited with 1 mW of 363 nm UV radiation and measured with a resolution of 0.1 nm. Multiplying the PL profile $F^{PL}(\lambda)\,\Delta\lambda$ (Fig. 3) by 1 mW and by the geometric factor of 4.2, then dividing by the spectral resolution $\Delta\lambda = 0.1$ nm yields the spectral PL $\dot{N}^{PL}(\lambda)$ of red algae calcite, emitted in all directions, shown in Fig. 10 (above). Integrating the result by summing the count rates for each wavelength in the 400 to 700 nm range with $\Delta\lambda = 1$ nm yields 6.12×10^7 photons per second with a standard deviation of 74,900 photons per second for the visible PL. The incident 363 nm laser radiation of 1 mW yields 1.83×10^{15} photons per second of the 363 nm photons. This shows that the probability that an incident UV photon will be absorbed and a PL photon emitted is 3×10^{-8}.

This first calculation yielded the result for extant red algae. It is assumed that the luminescent centers are of the same nature in trilobites. This calculation for trilobites assumes that both α and β are equal to 1. As described earlier, the value of α can be adjusted by moving the object to bring more or less scattered and reflected light into the aperture of the trilobite's eye. Considering β next, if the effective numerical aperture of the trilobite's eye for PL light is the same as that of the experiments of Pedone et al. (1990) and if the radiative rates and concentration of PL centers in the calcite of both trilobites and red algae are the same, then $\beta_1 = 1$ and $\beta_2 = 1$, respectively. If these quantities are different, then the appropriate value of $\beta = \beta_1\beta_2$ can be calculated. With these assumptions, both $\dot{N}^{PL}_{eye,tot}(d)$ and $\dot{N}^{solar}_{eye,tot}(d)$ can be calculated.

In the second calculation for the trilobite, the scaled obscuration factor $\varphi_{scaled}(d)$ for both the white and brown objects are calculated at the 3 ocean depths. By definition, φ_{scaled} is 1 at a depth of 1 cm. Its values at 1 m and 10 m show how the contrast of the trilobite's vision changed with depth. This second calculation has the advantage that it is independent of both unknown parameters α and β. This calculation has the further advantage that both the PL and solar photon count rates can be calculated based on well-established theoretical principles of optics. The 2 photon count rates are independent of each other, and their relative sizes are unimportant in this theoretical calculation.

Evaluating Equation (10) yielded the total power (mean and standard deviation) in the UV-A between 300 and 400 nm, P^{UV-A}_{tot}, to be $(2.10 \pm 0.03) \times 10^{-6}$ W, $(7.95 \pm 0.14) \times 10^{-7}$ W, and $(2.09 \pm 0.05) \times 10^{-10}$ W at depths of 1 cm, 1 m, and 10 m, respectively, for the white object. The respective values for the brown object are $(1.53 \pm 0.03) \times 10^{-7}$ W, $(5.69 \pm 0.10) \times 10^{-8}$ W, and $(1.41 \pm 0.04) \times 10^{-11}$ W. Combining these values for P^{UV-A}_{tot} with the measured photoluminescence profile $F^{PL}(\lambda)$ yielded the PL spectra divided by $\alpha\beta$ for those 3 depths, as shown in Fig. 11. Note that photon counting experiments obey Poisson statistics, for which the uncertainty of a measurement of N photons is given by $N^{1/2}$. Fig. 11 shows that the PL signal for UV-A reflected from the white object is notably stronger than the signal for the brown object, as expected.

The signal-to-noise ratios for 1 cm and 1 m depths for the white object show a clear signal in Fig. 11. The spectra for the brown object shows a reasonable signal-to-noise ratio for those 2 depths. The spectra at 10 m for both the white and brown objects shows a relatively poor signal-to-noise ratio. However, there are 301 data points in the visible spectra. Adding the count rates in all 301 channels yields a better signal-to-noise ratio for the overall count rate since its standard deviation is the square root of the sum of the variances.

The values of

$$\dot{N}^{PL}_{eye,tot} \Big/ \alpha\beta \qquad \text{and} \qquad \dot{N}^{solar}_{eys,tot} \Big/ \alpha$$

are determined from Equations (12) and (6), respectively, and are given in Table 2. These values permit an estimation of the total count rates for both the PL photons and the solar photons. Fig. 12 shows the scaled obscuration factor for both the white and brown objects. As shown by Equation (6), the total number rate of observed solar photons $\dot{N}^{solar}_{eye,tot}$ depends on the unknown parameter α. In order to determine its depth dependence, $\dot{N}^{solar}_{eye,tot}$ at 1 m and 10 m depth is divided by its value at 1 cm depth:

$$\dot{N}^{solar}_{eye,tot_{scaled}}(d) = \frac{\dot{N}^{solar}_{eye,tot}(d)}{\dot{N}^{solar}_{eye,tot}(0.01\ \text{m})} \tag{15}$$

The much lower reflectance of the brown object (see Fig. 6) is evident in the much lower count rate for the brown object, as shown in Table 2.

DISCUSSION AND SUMMARY

The result of the current work is that red algae calcite has a probability of about 3×10^{-8} for the photoluminescence process of absorbing a 363 nm photon followed by the emission of a visible photon, showing that this process is inefficient. This raises the possibility that the PL in its calcite would not have been observable by the trilobite since it might have been insignificant compared to the noise in the visible photons coming directly from the illuminated objects.

As discussed earlier, trilobites and red algae likely used similar biogenic processes to produce calcite crystals. The PL centers in red algae have been

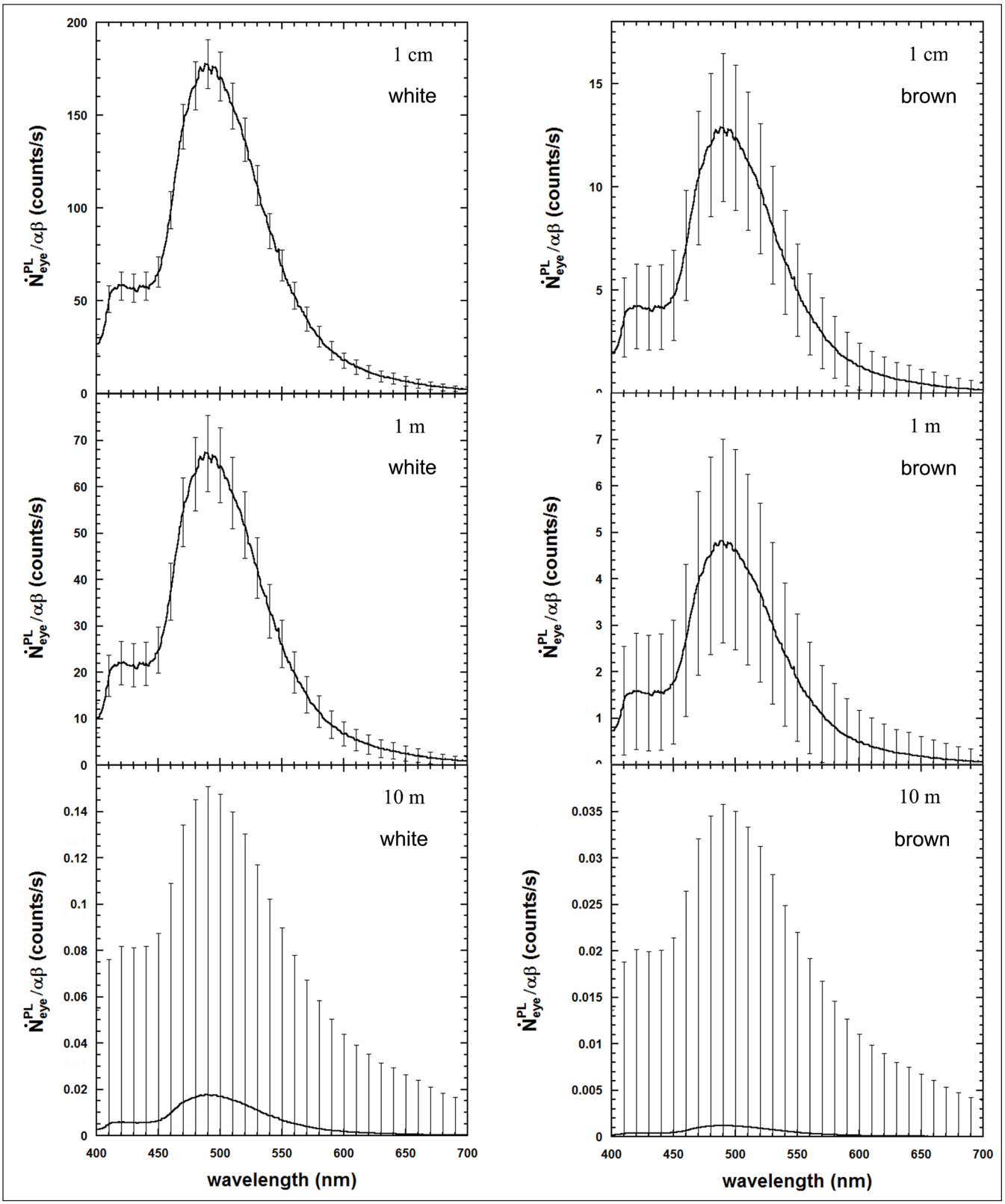

FIGURE 11. The observed PL photon count rate divided by αβ as a function of wavelength in the PL present in the calcite of the eyes of trilobites at the depths of 1 cm, 1 m, and 10 m for both the white and brown objects. The error bars are 1 standard deviation. Every tenth error bar is shown for clarity.

Table 2
The calculated parameters for ocean depths of 1 cm, 1 m, and 10 m

Parameter	Value					
	Object: white			Object: brown		
	Depth (m)			Depth (m)		
	0.01	1	10	0.01	1	10
$\dot{N}^{PL}_{eye,tot}/_{\alpha\beta}$ (counts/s)	18,494 ± 136	7,000 ± 84	1.84 ± 1.36	1,341 ± 37	501 ± 22	0.124 ± 0.353
$\dot{N}^{solar}_{eye,tot}/_{\alpha}$ (counts/s)	(2.95 ± 0.02) × 10^{13}	(2.60 ± 0.02) × 10^{13}	(1.54 ± 0.02) × 10^{13}	(2.52 ± 0.02) × 10^{12}	(2.12 ± 0.02) × 10^{12}	(1.07 ± 0.01) × 10^{12}
$\frac{\varphi(d)}{\varphi(0.01\ \mathrm{m})}$	1.000 ± 0.015	0.429 ± 0.008	(1.92 ± 1.41) × 10^{-4}	1.000 ± 0.010	0.444 ± 0.024	(2.19 ± 6.20) × 10^{-4}
$\frac{\dot{N}^{solar}_{eye,tot}(d)}{\dot{N}^{solar}_{eye,tot}(0.01\ \mathrm{m})}$	1.000 ± 0.010	0.883 ± 0.009	0.521 ± 0.005	1.000 ± 0.010	0.841 ± 0.009	0.424 ± 0.005

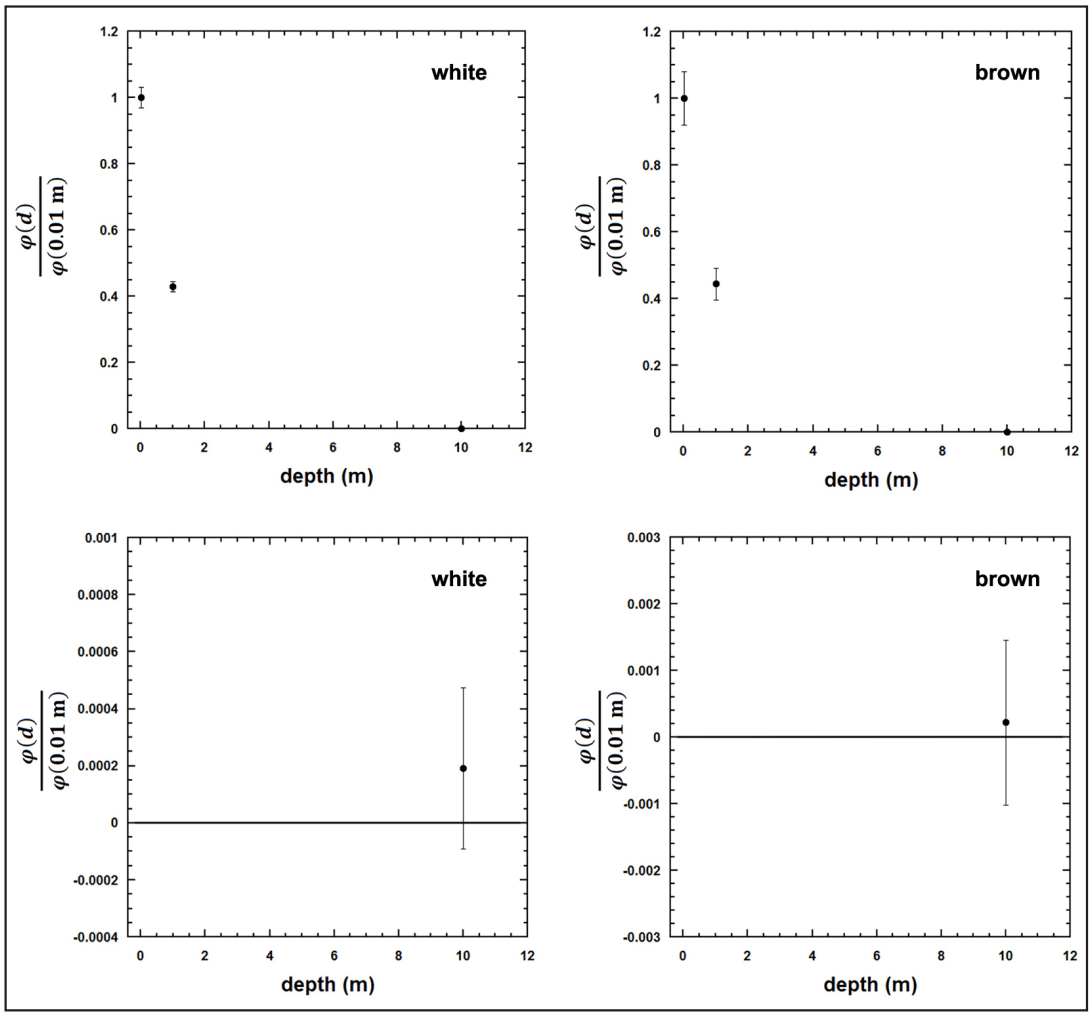

FIGURE 12. The scaled obscuration factor φ_{scaled} is shown for both the white object (left) and the brown object (right) as a function of ocean depth. The error bars show 2 standard deviations.

associated with carbon impurities in the calcite. These impurities are likely cellular components. Noting that the cells of trilobites might have been smaller than in red algae (since the general trend is that animals have smaller cells than plants), it is expected that the concentration of PL centers was different than in extant red algae. It is unlikely, however, that the concentration differed by more than 1 or 2 orders of magnitude.

Table 2 shows that for the white object at a depth of 1 cm (the object with the strongest PL signal),

$$\dot{N}^{PL}_{eye,tot} \Big/ \alpha\beta = 18{,}494 \pm 136 \text{ photons/s and}$$

$$\dot{N}^{solar}_{eye,tot} \Big/ \alpha = (2.95 \pm 0.02) \times 10^{13} \text{ photons/s.}$$

For a comparison of these 2 count rates, the value of α is irrelevant since both are divided by α. If $\beta = 1$, then the noise in the total solar count rate is about 7 orders of magnitude greater than the total PL count rate. The total PL count rate scales with β, which is expected to be no larger than 10 to 100. Assuming that $\beta = 100$, the total PL count rate is still insignificant (approximately 10^{-5}) in comparison to the noise of the total solar count rate. This implies that trilobites would not have been able to perceive the PL induced in the calcite of their eyes, making its presence irrelevant.

If a calcite crystal was recovered from a trilobite, PL could be excited from it by employing the same laser technique as that of Pedone et al. (1990) in their study of red algae calcite. These experiments would reveal the nature and concentration of the PL centers in trilobite calcite. Additional PL data could be taken by using a monochromator to create a beam of UV-A radiation with a narrow wavelength range from a wide band source. The monochromator could then be used to scan the wavelength range from 300 nm to 400 nm for measurement of the PL induced by different excitation wavelengths. Such experiments would test the predictions of the current study.

If β for trilobites was much larger than expected, then the PL in its calcite could have been perceived and lowered the contrast in its vision. In order to eliminate the reliance on an assumed value of β, the results for the current study's calculations of the scaled obscuration factor $\varphi_{scaled}(d)$ as a function of ocean depth will now be discussed. As suggested by Schoenemann et al. (2015), the amount of UV-A light penetrating to a certain ocean depth diminishes more quickly than the amount of visible light. This would manifest itself in a scaled obscuration factor φ_{scaled} which decreases with depth. Fig. 12 and Table 2 show that the scaled obscuration factor for both the white and brown objects display the expected behavior with depth. The lower panels of Fig. 12 show that the 2 standard deviation error bars of the scaled obscuration factor at an ocean depth of 10 m overlap with zero. This means that the PL in the eye of the trilobite is not degrading the contrast of its vision in any measurable manner—providing theoretical support to the suggestion of Schoenemann et al. (2015). Table 3 gives the statistical analysis of this decrease both in terms of the number of standard deviations different (the common form used in physics and astronomy) and in terms of the *p*-value (used in paleontology and biology). This table shows that the observed decreases are statistically significant.

Fig. 13 and Table 2 both show that the mean value of $\dot{N}^{solar}_{eye,tot\,scaled}$ decreases with depth, as expected. Because of the very high count rates for the observed solar photons, the uncertainties are very small. With an increase of depth from 1 cm to 10 m, the observed solar photon rates drop to 52.1 ± 0.6% for the white object and

Table 3
Statistical evaluation of observed decrease in the scaled obscuration factor $\frac{\varphi(d)}{\varphi(0.01\text{ m})}$

Pair	Number of standard deviations difference		*p*-value	
	White	Brown	White	Brown
1 cm to 1 m	24.8	8.73	$<3 \times 10^{-7}$	$<3 \times 10^{-7}$
1 m to 10 m	54.2	18.2	$<3 \times 10^{-7}$	$<3 \times 10^{-7}$
1 cm to 10 m	64.9	24.7	$<3 \times 10^{-7}$	$<3 \times 10^{-7}$

to 42.4 ± 0.5% for the brown object. It should be noted that, due to the difference in their reflectivity, the total observed solar count rate of the white object is about 11.7 times greater than observed for the brown object at a depth of 1 cm.

The natural variability of the illumination at the surface of the Earth is relevant to these calculations and can be examined on the basis of the power output of photovoltaic (PV) solar cell arrays. In solar cells, a solar photon absorbed in the depletion layer creates an electron-hole pair. The electric field of the depletion layer separates the electron and hole in opposite directions, forcing them through an external circuit where their energy is converted to do useful work. Their voltage is determined by the depletion layer, but their current is directly proportional to the number of photons striking the device per unit time. Since their energy is the product of the current and voltage, the energy produced by a solar cell is directly proportional to the number of photons per unit time incident on the solar cell—which is the quantity that must be evaluated.

Glass City Community Solar Inc. (GCSI 2023) kindly provided data from the 55.17 kW PV array located at 918 N. Michigan St. in Toledo, Ohio, for the days from July 7 to July 20, 2023 (inclusive). Their data were reported as the energy generated per hour. Note that an hour is a long time for observations of this variability, but such data also provide useful information considering that timescale. Fig. 14 shows the energy produced in the hour starting at 13:00 (1:00 PM) on each day. The largest amount was 42.030 kWh (on July 7), and the smallest was 3.939 kWh (on July 8). The energy produced on July 8 was 9.37% of the value for July 7. From this result, the natural variability observed by the PV array in a period of time of just 14 days is slightly larger than the amount shown in Fig. 13 and Table 2 for either the white or brown object. It might be assumed that trilobites evolved to be able to see adequately at all levels of illuminations found within the natural variability. This suggests, but does not prove, that the variability of $\dot{N}^{solar}_{eye,tot\,scaled}$ observed in this calculation would not have degraded its vision.

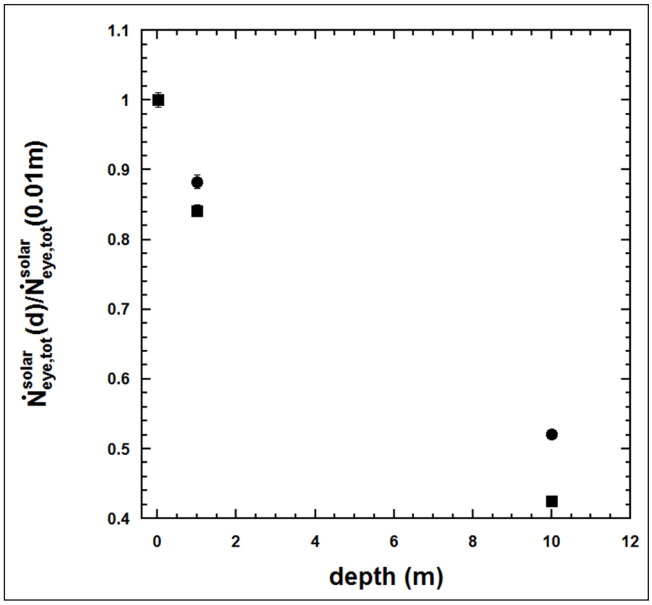

FIGURE 13. The scaled total solar count rate observed by the trilobite as a function of depth for the white object (solid black circles) and the brown object (solid black squares). Both are scaled to their total solar count rate at a depth of 1 cm. Note that the absolute total solar count rate at 1 cm is about 11.7 times higher for the white object than the brown object. The error bars are equal to 1 standard deviation.

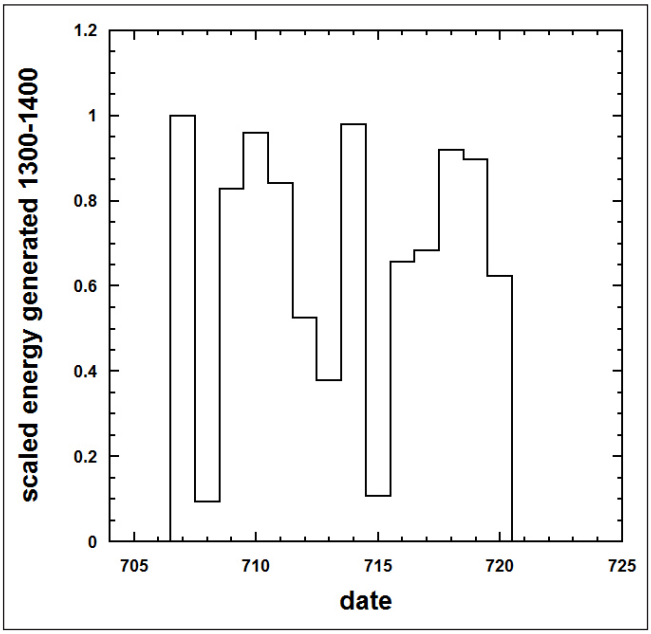

FIGURE 14. PV energy generated during the time from 13:00 to 14:00 hours on 14 different days in July 2023 by the 55.17 kW PV solar array located at 918 N. Michigan St. in Toledo, Ohio.

Conclusions

This theoretical study of trilobite vision provides evidence in support of the prediction of Schoenemann et al. (2015) that the relative amount of obscuring photoluminescence (PL) light diminishes with depth. Fundamentally, this result derives from the fact that UV-A light is absorbed more strongly than visible light by seawater and is independent of any model assumptions. The scaled obscuration factor $\varphi_{scaled}(d)$, which depends solely on measured quantities, is found to decrease with depth as the trilobite observes either a white or brown object. No significant PL light would have been observed by a trilobite at a depth of 10 m. These results suggest—but do not prove—that PL in the calcite of the eyes of trilobites was too small to be noticed by the animal at all depths. In fact, the PL appears to have been smaller than the noise in the total visible solar photons reflected and scattered by surrounding objects. These results also suggest that the PL in the calcite of the eyes of trilobites did not degrade their vision, particularly at depths below 1 m. Because the overall illumination decreases with depth, the natural variability in the sunlight at Earth's surface has been extracted from PV data. This analysis shows that trilobites would have been able to see at 10 m below the surface of the Paleozoic sea, particularly if imaging a white object.

These results are based on the model's assumptions that the sensitivity and spectral range of the trilobite's vision was the same as the extant marine crustacean *Squilla empusa* and that the spectral line shape of photoluminescence in the calcite of trilobites was the same as in extant red algae. If the sensitivity and spectral range of the trilobite's vision or the PL line shape were different from these assumptions, then the same general trend reported here (that the obscuring effect of the PL would have decreased with depth) would still hold, though with slightly different numbers.

ACKNOWLEDGEMENTS

Useful conversations with Lawrence Anderson-Huang, Mitra Dutta, and Randall Ellingson are gratefully acknowledged. Our thanks to Jakub Zalewski for drawing Figure 1 and to Mariusz Niechwedowicz for the photographs of the trilobite specimen in Figure 2. We thank the two anonymous referees whose constructive criticisms improved the manuscript significantly. We also thank the editors for their efforts.

LITERATURE CITED

Agatonovic-Kustrin S, Morton DW. 2012. The use of UV-visible reflectance spectroscopy as an objective tool to evaluate pearl quality. Mar Drugs. 10(7):1459-1475. https://doi.org/10.3390/md10071459

Armstrong FAJ, Boalch GT. 1961. The ultraviolet absorption of sea water. J Mar Biol Assoc UK. 41(3):591-597. https://doi.org/10.1017/S0025315400016179

Baer DR, Blanchard DL Jr. 1993. Studies of the calcite cleavage surface for comparison with calculation. App Surf Sci. 72(4):295-300. https://doi.org/10.1016/0169-4332(93)90365-I

Bergström J. 1973. Organization, life and systematics of trilobites. Fossils and Strata. 2:1-69. https://doi.org/10.18261/8200093301-1973-01

Bragg WL. 1924. The refractive indices of calcite and aragonite. P Roy Soc A-Math Phy. 105(732):370-386. https://doi.org/10.1098/RSPA.1924.0026

Brand U, Davis AM, Shaver KK, Blamey NJF, Heizler M, L´ecuyer C. 2021. Atmospheric oxygen of the Paleozoic. Earth-Sci Rev. 216:103560. https://doi.org/10.1016/j.earscirev.2021.103560

Brandt DS, Davis RA. 2007. Trilobites, Cincinnati, and the "Cincinnati School of Paleontology." In: Mikulic DG, Landing E, Klussendorf J, editors. Fabulous fossils—300 years of worldwide research on trilobites. Albany(NY): University of the State of New York, the State Education Department. New York State Museum Bulletin No. 507. p. 29-50. ISBN-13: 9781555572358.

Budde W. 1976. Calibration of reflectance standards. J Res NBS A Phys Ch. 80A(4):585-595. https://doi.org/10.6028/jres.080A.057

Clarkson ENK. 1979. The visual system of trilobites. Palaeontology. 22(1):1-22. https://biostor.org/reference/165366

Clarkson ENK, Levi-Setti R, Horvath G. 2006. The eyes of trilobites: the oldest preserved visual system. Arthropod Struct Dev. 35(4):247-259. https://doi.org/10.1016/j.asd.2006.08.002

Coleman HS. 1947. Stray light in optical systems. J Opt Soc Am. 37(6):434-451. https://doi.org/10.1364/JOSA.37.000434

Cooke GJ, Marsh DR, Walsh C, Black B, Lamarque J-F. 2022. A revised lower estimate of ozone columns during Earth's oxygenated history. Roy Soc Open Sci. 9(1):211165. https://doi.org/10.1098/rsos.211165

Cronin TW. 1985. The visual pigment of a stomatopod crustacean, *Sqilla empusa*. J Comp Physiol A. 156:679-687. https://doi.org/10.1007/BF00619117

Fan Q, Xu W, Hu X, Zhu W, Yue T, Zhang C, Yan F, Chen L, Lezec HJ, Lu Y, Agrawal A, Xu T. 2022. Trilobite-inspired neural nanophotonic light-field camera with extreme depth-of-field. Nat Commun. 13:2130. https://doi.org/10.1038/s41467-022-29568-y

Fordyce D, Cronin TW. 1993. Trilobite vision: a comparison of schizochroal and holochroal eyes with the compound eyes of modern arthropods. Paleobiology. 19(3):288-303. https://doi.org/10.1017/S0094837300000282

Fortey RA. 2004. The lifestyles of the trilobites. Am Sci. 92(5):446-453. https://doi.org/10.1511/2004.5.446

Fortey RA, Owens RM. 1999. Feeding habits in trilobites. Palaeontology. 42(3):429-465. https://doi.org/10.1111/1475-4983.00080

Gaft M, Nagli L, Panczer G, Waychunas G, Porat N. 2008. The nature of unusual luminescence in natural calcite $CaCO_3$. Am Mineral. 93(1):158-167. https://doi.org/10.2138/am.2008.2576

Gaft M, Reisfeld R, Panczer G. 2015. Modern luminescence spectroscopy of minerals and materials. 2nd ed. Cham (CH): Springer. p. 67-68. ISBN-13: 9783319247656. https://doi.org/10.1007/978-3-319-24765-6

GCSI. 2023. PV generation data for July 7 through July 20, 2023, was kindly provided by Glass City Community Solar Inc., Toledo, Ohio. Received on 2023 July 24.

Ghosh G. 1999. Dispersion-equation coefficients for the refractive index and birefringence of calcite and quartz crystals. Opt Commun. 163(1-3):95-102. https://doi.org/10.1016/S0030-4018(99)00091-7

Grabner M, Kvicera V. 2011. The wavelength dependent model of extinction in fog and haze for free space optical communication. Opt Express. 19(4):3379-3386. https://doi.org/10.1364/OE.19.003379

Hale GM, Querry MR. 1973. Optical constants of water in the 200-nm to 200-μm wavelength region. Appl Optics. 12(3):555-563. https://doi.org/10.1364/AO.12.000555

Horvath G. 1989. Geometric optics of trilobite eyes: a theoretical study of the shape of the aspherical interface in the cornea of schizochroal eyes of phacopid trilobites. Math Biosci. 96(1):79-94. https://doi.org/10.1016/0025-5564(89)90084-9

Jafari H, Khajeh Mehrizi M, Fattahi S. 2016. The effect of inorganic nanoparticles on camouflage properties of cotton/polyester fabrics. Prog Color Colorants Coat. 9(1):29-40. https://doi.org/10.30509/pccc.2016.75872

Jell PA. 1975. The abathochroal eye of *Pagetia*, a new type of trilobite eye. Foss Strata. 4:33-43. https://doi.org/10.18261/8200049639-1975-02

Karampelas S, Fritsch E, Gauthier JP, Hainschwang T. 2011. UV-Vis-NIR reflectance spectroscopy of natural-color saltwater cultured pearls from *Pinctada margaritifera*. Gems Gemol. 47(1):31-35. https://doi.org/10.5741/GEMS.47.1.31

Krause AJ, Mills BJW, Zhang S, Planavsky NJ, Lenton TM, Poulton SW. 2018. Stepwise oxygenation of the Paleozoic atmosphere. Nat Commun. 9:4081. https://doi.org/10.1038/s41467-018-06383-y

Lee MR, Torney C, Owen AW. 2012. Biomineralization in the Palaeozoic oceans: evidence for simultaneous crystallization of high and low magnesium calcite by phacopine trilobites. Chem Geol. 314-317:33-44. https://doi.org/10.1016/j.chemgeo.2012.04.033

Lepley LK, Adams WM. 1968. Reflectivity of electromagnetic waves at an air-water interface for pure and sea water. Honolulu (HI): Water Resources Research Center, University of Hawaii at Manoa. Technical Report No. 25, Geophysical exploration for Hawaiian groundwater, phase II. Report 1 of 4. 15 p. OWRR Project No.: B-008-HI. Grant Agreement No.: 14-01-0001-1494. https://hdl.handle.net/10125/7600

Lindström G. 1901. Researches on the visual organs of the trilobites. Stockholm (SE): Kongl Sven Vetensk-Akad Handl [Royal Swedish Academy of Sciences Transactions]. 34(8):6-74. https://catalog.hathitrust.org/Record/100445732

Lytle JD, Morrow HE, editors. 1977. Stray light problems in optical systems. Proceedings of the 1977 SPIE/SPSE Technical Symposium East; 1977 April 18-21; Reston, Va. Bellingham (WA): SPIE (Society of Photo-Optical Instrumentation Engineers). 184 p. SPIE Proceedings, Vol. 107.

McClatchey RA, Fenn RW, Selby JEA, Volz FE, Garing JS. 1971. Optical properties of the atmosphere (revised). Bedford (MA): Air Force Cambridge Research Laboratories. 98 p. Environmental Research Papers, Report No.: 354. Project No.: 7670-09-01. Sponsored by: Air Force Cambridge Research Laboratories, Hanscom Field, Bedford, Ma. Originators Report No.: AFCRL-71-0279. https://catalog.hathitrust.org/Record/102325589

McCormick T, Fortey RA. 1998. Independent testing of a paleobiological hypothesis: the optical design of two Ordovician pelagic trilobites reveals their relative paleobathymetry. Paleobiology. 24(2):235-253. https://doi.org/10.1666/0094-8373(1998)024[0235:ITOAPH]2.3.CO;2

[NREL] National Renewable Energy Laboratory. 2023. Reference air mass 1.5 spectra. Washington (DC): US Department of Energy, Office of Energy Efficiency and Renewable Energy, National Renewable Energy Laboratory; [accessed 2023 June 29]. https://www.nrel.gov/grid/solar-resource/spectra-am1.5.html

Pedone VA, Cercone KR, Burruss RC. 1990. Activators of photoluminescence in calcite: evidence from high-resolution, laser-excited luminescence spectroscopy. Chem Geol. 88(1-2):183-190. https://doi.org/10.1016/0009-2541(90)90112-K

Ribas I. 2009. The Sun and stars as the primary energy input in planetary atmospheres. In: Kosovichev AG, Andrei AH, Rozelot JP, editors. Solar and Stellar Variability: Impact on Earth and Planets. Proceedings of the 264th Symposium of the International Astronomical Union, Volume 5; 2009 Aug 3-7; Rio de Janeiro, Brazil. Cambridge (UK): Cambridge University Press. p. 3-18. https://doi.org/10.1017/S1743921309992298

Rudkin DM, Young GA, Elias RJ, Dobrzanski EP. 2003. The world's biggest trilobite–*Isotelus rex* new species from the Upper Ordovician of northern Manitoba, Canada. J Paleontol. 77(1):99-112. https://doi.org/10.1666/0022-3360(2003)077<0099:TWBTIR>2.0.CO;2

Schoenemann B. 2021. An overview on trilobite eyes and their functioning. Arthropod Struct Dev. 61:101032. https://doi.org/10.1016/j.asd.2021.101032

Schoenemann B, Clarkson ENK, Ahlberg P, Alvarez MED. 2010. A tiny eye indicating a planktonic trilobite. Palaeontology. 53(4):695-701. https://doi.org/10.1111/j.1475-4983.2010.00966.x

Schoenemann B, Clarkson ENK, Bartels C, Südkamp W, Rössner GE, Ryck U. 2021. A 390 million-year-old hyper-compound eye in Devonian phacopid trilobites. Sci Rep. 11:19505. https://doi.org/10.1038/s41598-021-98740-z

Schoenemann B, Clarkson ENK, Horváth G. 2015. Why did the UV-A-induced photoluminescent blue-green glow in trilobite eyes and exoskeletons not cause problems for trilobites? PeerJ. 3:e1492. https://doi.org/10.7717/peerj.1492

Toffolo MB, Ricci G, Caneve L, Kaplan-Ashiri I. 2019. Luminescence reveals variations in local structural order of calcium carbonate polymorphs formed by different mechanisms. Sci Rep. 9:16170. https://doi.org/10.1038/s41598-019-52587-7

Whitfield J. 2001. Eyes in their stars. Nature. https://doi.org/10.1038/news010823-11

Whittington HB. 1992. Trilobites. Woodbridge (UK): Boydell Press. 145 p. In series: Fossils Illustrated, vol. 2. ISBN-13: 9780851153117.

Wilmot NV, Fallick AE. 1989. Original mineralogy of trilobite exoskeletons. Palaeontology. 32(2):297-304. https://www.biodiversitylibrary.org/part/173949 or https://biostor.org/reference/165863

Woźniak B, Dera J. 2007. Light absorption in sea water. In: Mysak LA, Hamilton K, editors. Atmospheric and oceanographic sciences library, vol. 33. New York(NY): Springer Science and Business Media. 450 p. ISBN-13: 9780387307534 https://doi.org/10.1007/978-0-387-49560-6